Congenital Myasthenic Syndrome Caused by Decreased Agonist Binding Affinity Due to a Mutation in the Acetylcholine Receptor ϵ Subunit

Kinji Ohno,* Hai-Long Wang,† Margherita Milone,* Nina Bren,† Joan M. Brengman,* Satoshi Nakano,* Polly Quiram,† Jerry N. Pruitt,* Steven M. Sine,† and Andrew G. Engel*
*Muscle Research Laboratory
Department of Neurology
†Receptor Biology Laboratory
Department of Physiology and Biophysics
Mayo Foundation
Rochester, Minnesota 55905

Summary

We describe the genetic and kinetic defects for a low-affinity fast channel disease of the acetylcholine receptor (AChR) that causes a myasthenic syndrome. In two unrelated patients with very small miniature end plate (EP) potentials, but with normal EP AChR density and normal EP ultrastructure, patch-clamp studies demonstrated infrequent AChR channel events, diminished channel reopenings during ACh occupancy, and resistance to desensitization by ACh. Each patient had two heteroallelic AChR ϵ subunit gene mutations: a common ϵP121L mutation, a signal peptide mutation (ϵG-8R) (patient 1), and a glycosylation consensus site mutation (ϵS143L) (patient 2). AChR expression in HEK fibroblasts was normal with ϵP121L but was markedly reduced with the other mutations. Therefore, ϵP121L defines the clinical phenotype. Studies of the engineered ϵP121L AChR revealed a markedly decreased rate of channel opening, little change in affinity of the resting state for ACh, but reduced affinity of the open channel and desensitized states.

Introduction

Increasing evidence supports the notion that a kinetic abnormality of the acetylcholine receptor (AChR) in a congenital myasthenic syndrome (CMS) predicts a mutation in one or more AChR subunits (Engel, 1994b; Ohno et al., 1995a; Sine et al., 1995b). Thus, we showed that prolonged activation of the AChR channel in the slow-channel CMS is associated with mutations in the M2 and even the M1 transmembrane domains (Ohno et al., 1995a; Ohno et al., 1995b; Ohno et al., 1996), or with a mutation in the extracellular domain of the α subunit that increases the affinity of AChR for acetylcholine (ACh) (Sine et al., 1995b). We now report discovery of a mutation in the ϵ subunit gene in two unrelated patients that results in abnormally infrequent and brief episodes of channel activation. We show that these effects are attributable to a decreased affinity of AChR for ACh, as well as a decreased rate of channel opening. Our findings illustrate the importance of the affinity of AChR for ACh in governing both the efficiency and time course of the synaptic response, and reconfirm the crucial role of the ϵ subunit in ACh binding.

Results

Clinical Data

Patient 1 of this communication was previously reported in a description of a syndrome attributed to abnormal interaction of acetylcholine (ACh) with AChR (Uchitel et al., 1993). In brief, this woman, now 28 years old, had moderately severe myasthenic symptoms since birth. Studies of an intercostal muscle specimen at age 21 revealed normal end plate (EP) ultrastructure, normal number of AChR per EP, and normal evoked quantal release, but very small miniature EP potentials (MEPPs). Analysis of ACh-induced current noise was best fitted by a double Lorentzian, suggesting a kinetic abnormality of AChR or two populations of AChRs at the EPs (Uchitel et al., 1993). The parents, two siblings, and two children are unaffected. Patient 2, a 4 year-old boy, has also had myasthenic symptoms present since birth. His parents are unaffected, but a younger sister has elements of the same disease. Both patients had negative tests for anti-AChR antibodies and decremental compound muscle action potential responses on 2 Hz nerve stimulation, and responded incompletely to anticholinesterase drugs.

Electrophysiologic and Morphologic Studies in Patient 2

MEPPs were of such low amplitude that many were lost in the baseline noise. Normally, *d*-tubocurarine is required to prevent muscle twitching during recording of end plate potentials (EPPs), but in the patient, EPPs could be recorded in its absence. In this 4 year-old patient, the quantal content of the EPP (*m*) fell in the lower range of values obtained in adult controls, but was higher than in a 3 year-old control patient (Table 1). The amplitude of the MEPPs, calculated from the quantal component of the EPP (Elmqvist and Quastel, 1965), was markedly reduced (Table 1). Despite the small amplitude of the MEPP, the number of end plate EP-specific α-bungarotoxin (α-bgt)- binding sites was 5.2×10^6 per EP. This value was higher than in a 3 year-old control subject (4.7×10^6) but lower than in 13 adult controls ($12.82 \pm 2.84 \times 10^6$; mean ± SD). When EP AChR was visualized in frozen sections with rhodamine-labeled α-bgt, the intensity of the fluorescent signal was comparable with that observed at control EPs. Ultrastructural localization of AChR with peroxidase-labeled α-bgt revealed a normal density and distribution of AChR on the crests of the junctional folds (Figure 1), and the AChR index (defined as the ratio of the length of the postsynaptic membrane reacting for AChR to the length of the primary synaptic cleft [Engel, 1994a]) was 3.11 ± 1.44 (mean ± SE; 24 EP regions). This value is close to the range of means obtained in five control subjects (3.13–3.31).

Ultrastructural examination of 30 regions of 14 EPs

Table 1. Analysis of MEPPs and Quantal Content of EPP

	15 Adult Controls	Patient 2
m[a]	31 ± 14 (190)[b]	22 ± 7 (30)
MEPP Amplitude (mV)	1.00 ± 0.32 (165)	0.067 ± 0.031 (30)[c]

Values indicate mean ± SD. Measurements at 29°C ± 0.5°C. Number of EPs are indicated in parentheses.

[a] Quantal content of EPP at 1 Hz stimulation corrected for a resting membrane potential of −80 mV, nonlinear summation, and non-Poisson release.

[b] In a 3 year-old control patient *m* was 18 ± 7 (18).

[c] Estimated by dividing the corrected EPP amplitude by *m*, and corrected for a fiber diameter of 50 μm.

showed no qualitative abnormality (Figure 1). Morphometric analysis of these EPs demonstrated normal postsynaptic membrane density and normal synaptic vesicle diameters (data not shown). The electrophysiologic and morphologic findings in patient 2, which were similar to those previously reported in patient 1 (Uchitel et al., 1993), suggested an abnormal interaction of AChR with ACh.

Patch-Clamp Analysis of EP AChR Channels in Patient 2

To search for a kinetic defect of AChR, we recorded single-channel currents from the EPs of the patient in the presence of 50 nM to 50 μM ACh. Channel openings were not detected at 50 nM ACh, were infrequent with 0.1 μM ACh, and were less frequent than normal with 1 μM ACh (Figure 2). At 1 μM ACh, the channel open intervals had a major component that was shorter than the major component of normal open intervals, and a minor component of similar duration to that of the major component of normal open intervals (Table 2). Channel open intervals, burst durations, and relative areas were essentially unaltered at ACh concentrations ranging from 50 nM to 20 μM. At 50 μM ACh, the minor component of channel open intervals was absent. It was notable that channel openings showed resistance to clustering with increasing concentrations of ACh and clusters of openings were detected only in the presence of 50 μM ACh, whereas at normal EPs, such clusters appear with ACh concentrations greater than 1 μM. The opening episodes were seldom interrupted by brief closures, so that the major component of the burst open duration was not significantly longer than that of the open intervals, but was significantly shorter than the major component of the burst open duration at control EPs (Figure 2; Table 2). Channel events from the EP of the patient, as in more than 99% of channel events at normal EPs, had a conductance of ca. 60 pS. Approximately 7% of events at the EPs of the patient had a reduced conductance of ca. 46 pS and prolonged open durations typical of AChRs containing the γ instead of the ε subunit (Mishina et al., 1986). That the major ACh-evoked channel events occurred at a reduced frequency, had abnormally brief bursts of openings, and were resistant to clustering at high concentrations of ACh pointed to a kinetic defect in AChR.

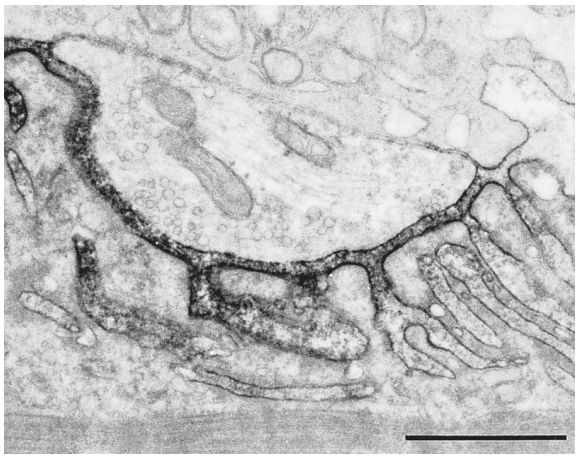

Figure 1. Ultrastructural Localization of EP AChR with Peroxidase-Labeled α-bgt

The density and distribution of AChR on the junctional folds is normal. Scale bar represents 1 μm.

Mutational Analysis in Patient 1

In this patient, the very low MEPP amplitude without EP AChR deficiency (Uchitel et al., 1993) prompted us to search for a mutation in one or more AChR subunits. We first screened for mutations by single-strand conformation polymorphism (SSCP) analysis on PCR-amplified fragments of genomic DNA encoding the α, β, δ, and ε subunits. We detected six aberrant conformers; five were commonly observed even in normal controls, but one was unique to patient 1. Direct sequencing of the corresponding DNA fragments identified five heterozygous polymorphisms: α130–13insT in α intron 2; δG57A in δ exon 2, causing no amino acid substitution; εC857+15G in ε intron 8; εC973–6T in ε intron 9; and εC1233T in ε exon 11, causing no amino acid substitution.

The aberrant conformer unique to patient 1 was due to a heterozygous C-to-T transition in ε exon 5 at nucleotide 362 (εC362T) that converted a proline to a leucine codon at position 121 (εP121L) (Figure 3A). The altered proline is located in the extracellular domain of the ε subunit and is conserved across all subunits and species (Figure 4).

To check for mutations that SSCP analysis might have missed, we sequenced all exons and flanking intronic regions of the α, β, δ, and ε subunits. This revealed another heterozygous polymorphism, εG-8T in ε exon 2, predicting an εG-3V substitution in the signal peptide region, as well as a εG-24A mutation in ε exon 1 that converts a glycine to an arginine codon at position −8 (εG-8R) in the signal peptide region (Figure 3A). The altered glycine at −8 is not conserved among the other human subunits nor among the ε subunits of other species.

εP121L resulted in loss of a MspI restriction site. MspI digestion of DNA samples obtained from family members revealed that mother and son of patient 1 also carry εP121L (Figure 3B). A search for εG-8R by allele-specific PCR showed that the father and daughter of patient 1 are heterozygous for εG-8R (Figure 3B). Allele-specific PCR also established that patient 1 inherited the εG-3V polymorphism from her mother (data not shown). Since

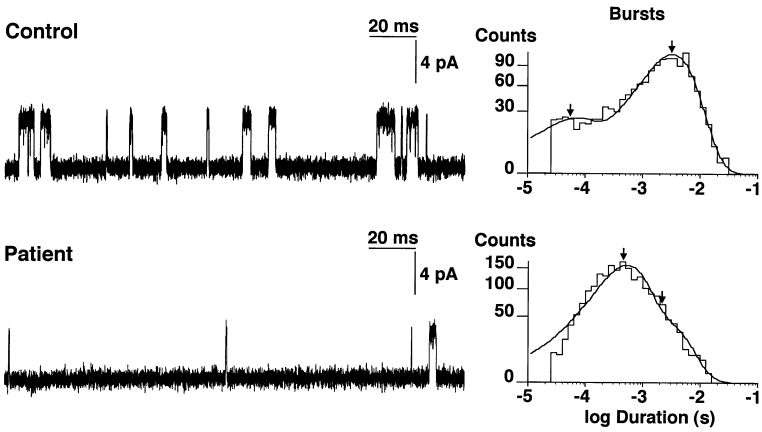

Figure 2. Channel Events Elicited by 1 μM ACh at a Control EP and at an EP of Patient 2

Channel openings (shown as upward deflections) are less frequent and the dominant component of openings is briefer in the patient than in the control. Logarithmically binned burst duration histograms are fitted by the sum of exponentials. Time constant, τ_n and relative areas, α_n, for each component of bursts: Control: τ_1 = 0.05 ms, a_1 = 0.14, τ_2 = 3.24 ms, a_2 = 0.88, total events, 1444. Patient 2: τ_1 = 0.46 ms, a_1 = 0.77, τ_2 = 2.1 ms, a_2 = 0.23, total events, 2046. −80 mV, T = 22°C ± 0.5°C.

the polymorphism and mutation of the signal peptide in patient 1 reside on different alleles, the polymorphism does not contribute to the pathogenic effects of the mutation. Restriction analysis for ϵP121L and allele-specific PCR for ϵG-8R revealed no similar mutations in 100 normal controls or in 42 unrelated CMS patients.

Mutational Analysis in Patient 2

In this patient, the patch-clamp evidence for a kinetic defect in AChR, as well as the low MEPP amplitude without EP AChR deficiency pointed to a mutation in an AChR subunit. Since the low MEPP amplitude without EP AChR deficiency was like that in patient 1, we first searched for ϵP121L detected in patient 1. Indeed, MspI restriction analysis of genomic DNA in patient 2 confirmed that he also harbors a heterozygous ϵP121L mutation. We then searched for a second mutation in the ϵ subunit by sequencing all exons and adjacent intronic regions of the ϵ subunit gene. This revealed two heterozygous polymorphisms (ϵC-60–70T, 70 bases upstream from the first base of the translational start site, and ϵA1245G in exon 11 causing no amino acid substitution), as well as a second mutation. The second mutation was a heterozygous C-to-T transition at nucleotide 428 in ϵ exon 5 that converts a serine to a leucine codon at position 143 (ϵS143L) (Figure 3A). The altered serine is part of a consensus sequence for N-glycosylation at N141 (Gehle and Sumikawa, 1991) and is conserved (Figure 4). The corresponding amino acid in the human β subunit is threonine, which also signals for glycosylation (Figure 4).

Restriction analysis with MspI revealed the ϵP121L mutation not only in patient 2, but also in his asymptomatic mother and symptomatic sister (Figure 3C) and allele-specific PCR demonstrated the ϵS143L mutation in his asymptomatic father and his symptomatic sister (Figure 3C). ϵS143L was not found in 100 normal controls or in 42 unrelated CMS patients.

To summarize, both patients have two heterozygous and heteroallelic ϵ subunit gene mutations. Both patients share ϵP121L; patient 1 also has a signal peptide mutation (ϵG-8R) and patient 2 a glycosylation consensus site mutation (ϵS143L). Therefore, we designed expression studies to determine the effects of the mutations on the expression, ACh-binding affinity, and kinetic properties of AChR.

Expression Studies of Mutant ϵ Subunits

Our molecular genetic analysis suggests that ϵP121L plus either ϵG-8R or ϵS143L are required to produce disease (Figure 3). To test this hypothesis further, we engineered each mutation into the human ϵ subunit and coexpressed each with complementary α, β, and δ subunits in 293 HEK cells. As a control, we coexpressed α, β, and δ subunits in the absence of the ϵ subunit. Measurements of ^{125}I-α-bgt binding revealed robust expression of wild-type and ϵP121L AChRs, but reduced expression in the presence of ϵG-8R, ϵS143L, or in the absence of the ϵ subunit (Figure 5A).

To determine whether the residual α-bgt binding in the presence of ϵG-8R or ϵS143L can be accounted for by $\alpha_2\beta\delta_2$ pentamers, we measured ACh binding by competition against the initial rate of ^{125}I-α-bgt binding

Table 2. Open Intervals and Bursts of 60 pS Channels at Control End Plates and at End Plates of Patient 2

	Open Intervals		Bursts	
	Controls	Patient 2	Controls	Patient 2
τ_1 (ms)	0.07 ± 0.02	0.38 ± 0.04	0.09 ± 0.03	0.45 ± 0.04
Area	0.14 ± 0.04	0.86 ± 0.03	0.13 ± 0.02	0.83 ± 0.03
Number of EPs	7	7	7	7
τ_2 (ms)	1.13 ± 0.10	1.69 ± 0.14	2.99 ± 0.26	2.48 ± 0.50
Area	0.86 ± 0.04	0.16 ± 0.02	0.87 ± 0.02	0.17 ± 0.03
Number of EPs	7	6[a]	7	7

Values indicate means ± SE. ACh concentration = 1 μM. Potential = −80 mV; T = 22°C ± 0.5°C.
[a] The second and minor component of open intervals and bursts was not present at all patient EPs.

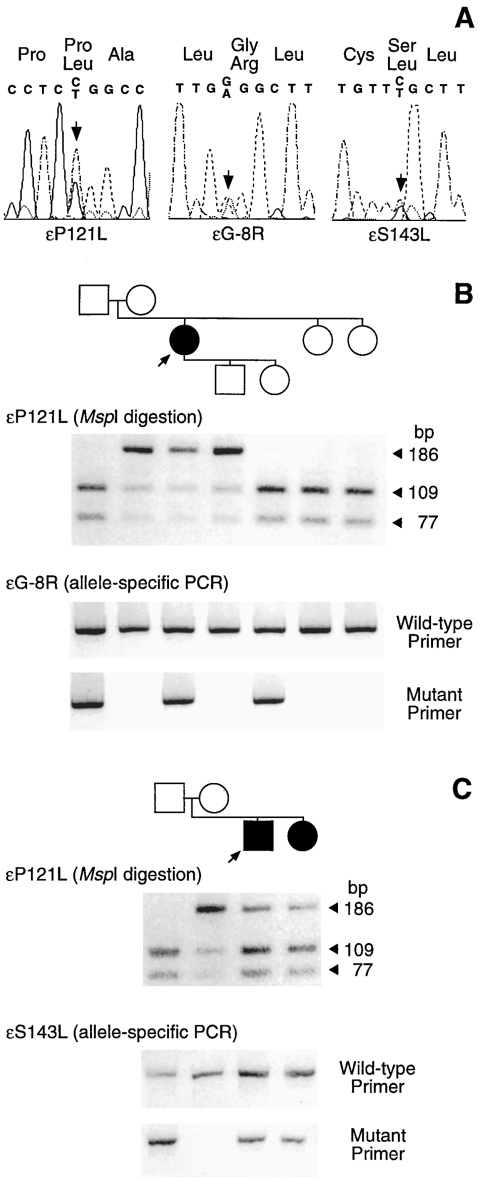

Figure 3. Identification and Molecular Genetic Analysis of Mutations in AChR ε Subunits

(A) Automated sequencing of ε exon 5 around codon 121 in patient 1 (left panel), ε exon 1 around codon −8 in patient 1 (middle panel), and ε exon 5 around codon 143 in patient 2 (right panel). The double peaks showing heterozygous mutations are indicated by arrows. The deduced amino acids are shown at the top.

(B) Upper panel: MspI restriction analysis of genomic DNA in the family of patient 1. For the εP121L mutation, the wild-type allele yields 77- and 109-bp fragments; the mutant allele gives rise to a 186-bp fragment. Both wild-type and mutant fragments are present in patient 1 and in her asymptomatic mother and son. Lower panels: Allele specific PCR demonstrates the εG-8R mutation in patient 1 and in her asymptomatic father and daughter.

(C) Upper panel: MspI restriction analysis of genomic DNA in the family of patient 2. The εP121L mutation is present in patient 2, his asymptomatic mother, and his symptomatic sister. Lower panels: Allele specific PCR demonstrates εS143L mutation in patient 2, his asymptomatic father, and symptomatic sister.

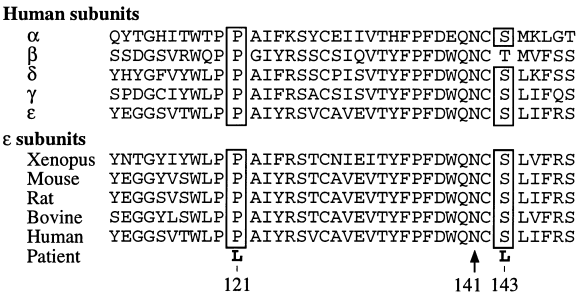

Figure 4. Multiple Alignment of Part of the Extracellular Domains of Muscle Nicotinic AChR

Proline 121 is strictly conserved in other human subunits and in the ε subunits of other species. Serine 143 is conserved in human α, δ, and γ subunits, and in the ε subunits of the other species. Boxes enclose the conserved amino acids. Arrow indicates N-glycosylation site at 141.

(Sine and Taylor, 1979). For $\alpha_2\beta\delta_2$ pentamers, ACh binding is biphasic with a plateau at 50% occupancy extending over three decades of ACh concentration (Figure 5B). This biphasic profile is similar to that described for mouse $\alpha_2\beta\delta_2$ pentamers (Sine and Claudio, 1991), and contrasts with that for $\alpha_2\beta\epsilon\delta$ pentamers that bind ACh cooperatively (see Figure 8B). When εS143L is cotransfected, ACh binding closely mimics that observed with α, β, and δ subunits alone, suggesting that all of the α-bgt binding corresponds to $\alpha_2\beta\delta_2$ pentamers (Figure 5B). When εG-8R is cotransfected, binding of ACh is again biphasic, but the amplitude of the plateau is reduced from 50% to approximately 25%. This asymmetric profile for εG-8R is well described as the sum of a monophasic profile similar to that of wild-type AChR, plus a biphasic profile corresponding to $\alpha_2\beta\delta_2$ pentamers. These results suggest that the ε subunit harboring S143L does not assemble with α, β, and δ subunits to form pentamers, but the ε subunit harboring G-8R assembles, although with markedly reduced efficiency.

To determine whether ε subunits containing G-8R or εS143L can assemble with complementary subunits, we studied their ability to oligomerize with the α subunit, the earliest step in AChR assembly. We determined the number of αε complexes from the number of curare-displaceable α-bgt sites in cells permeablized with saponin. The ε subunit containing the glycosylation mutation, S143L, fails to assemble with the α subunit, as the number of specific α-bgt binding sites is indistinguishable from that observed in the presence of the α subunit alone (Figure 5C). The ε subunit containing the signal peptide mutation, G-8R, produces about 10% of the αε complexes observed with wild-type ε. Thus, ε subunits containing εG-8R or εS143L incorporate with reduced efficiency into surface AChRs owing to impaired association with the α subunit. Therefore, in patients 1 and 2, the predominant surface AChR is likely to contain the εP121L mutation.

Comparison of EP and Engineered εP121L AChRs

To confirm pathogenicity of εP121L, we compared single-channel currents recorded from EPs of patient 2

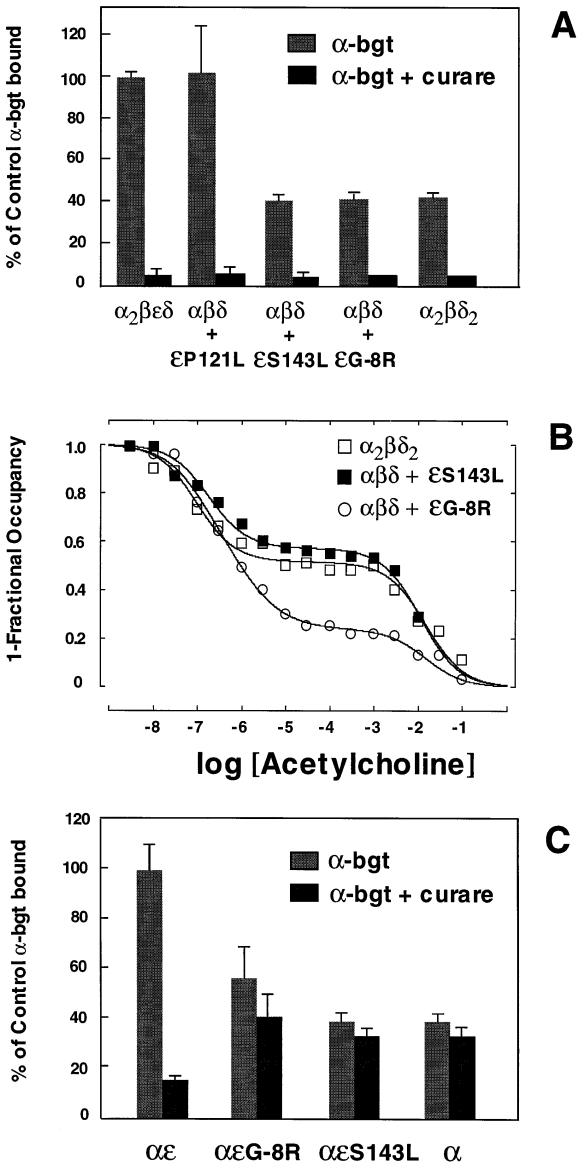

Figure 5. Expression of Mutant ϵ Subunits

(A) Total α-bgt binding to intact HEK cells transfected with the indicated AChR cDNAs. The amount of bound ^{125}I-α-bgt is normalized to that measured for the wild-type human AChR ($\alpha_2\beta\epsilon\delta$). Nonspecific binding is that measured in the presence of 300 μM *d*-tubocurarine (α-bgt + curare, closed bars).

(B) Acetylcholine binding to intact cells transfected with the indicated AChR cDNAs determined by competition against the initial rate of ^{125}I-α-bgt binding. For $\alpha_2\beta\delta_2$, the smooth curve is a fit to the two site equation (Equation 2) with $K_A = 9.6 \times 10^{-8}$, $K_B = 1.5 \times 10^{-2}$, and $fract_A = 0.48$. For $\alpha\beta\delta$ + ϵS143L, the curve is a two site fit with $K_A = 1.7 \times 10^{-7}$, $K_B = 1.2 \times 10^{-2}$, and $fract_A = 0.43$. For $\alpha\beta\delta$ + ϵG-8R, the curve is a weighted sum of the fit determined for $\alpha_2\beta\delta_2$ plus a component described by the Hill equation (Equation 1); the fitted parameters are: $K_{ov} = 7.6 \times 10^{-7}$, n = 0.8, and the fraction of sites corresponding to $\alpha_2\beta\delta_2$ equals 0.47.

(C) Total α-bgt binding to saponin-permeabilized cells transfected with the indicated pairs of AChR subunit cDNAs or with the α subunit alone. The amount of bound ^{125}I-α-bgt is normalized to that measured for wild-type αϵ dimers. Nonspecific binding is that measured in the presence of 300 μM *d*-tubocurarine (α-bgt + curare, closed bars).

with those from 293 HEK cells transfected with either wild-type or mutant human cDNAs. We chose a high concentration of ACh for this comparison because the essential defect in this syndrome is reduced response to ACh despite normal density of AChR at the EP. At 50 μM ACh, the wild-type AChR activates in clusters of openings, owing to repeated activation of a single channel, separated by prolonged closed periods due to desensitization; within a cluster, the mean probability of opening is high, 0.83 ± 0.06. In contrast, AChRs from both the patient EPs and HEK cells transfected with ϵP121L open with low probability within clusters (Figure 6). For AChRs at the EP of patient 2, the mean open probability within identified clusters is 0.081 ± 0.02 at 50 μM ACh, while that for the engineered ϵP121L mutant is 0.04 ± 0.01 at 200 μM ACh. We found that the engineered ϵP121L AChR required higher concentrations of ACh to approach the open probability of the AChR at the EP of the patient. Nevertheless, both the EP and engineered mutant AChRs open with markedly reduced efficiency.

Kinetic Steps in AChR Activation Affected by ϵP121L

To identify the kinetic steps affected by ϵP121L, we recorded single-channel currents over a range of ACh concentrations from 293 HEK cells transfected with either wild-type or mutant human cDNAs. As observed for AChR from other species, the human wild-type AChR opens in clusters of well defined activation episodes at concentrations of ACh greater than 3 μM (Figure 7A). By contrast, openings of the ϵP121L AChR appear as a steady stream of events at 3 μM ACh, and show only loose clustering at concentrations greater than 30 μM (Figure 7B). Both the wild-type and mutant AChR exhibit brief and long duration openings at 3 μM ACh, and only long duration openings at saturating concentrations; brief openings are visible as the component with a mean duration of about 40 μs at 3 μM that is not present at concentrations of 100 μM or greater (Figures 7A and 7B). For the wild-type AChR, closed intervals within clusters become progressively briefer with increasing ACh concentration, and at the highest concentrations approach the limit of resolution of the recording system (Figure 7A). For the ϵP121L AChR, closed intervals within clusters also become briefer with increasing ACh concentration, but their mean duration approaches a limit of about 10 ms (Figure 7B). These observations show that although ϵP121L does not affect the stability of the open channel (i.e., mean open duration), it markedly impairs both the rate of opening and the fraction of time spent in the open state.

To describe quantitatively activation of wild-type and mutant AChRs, we interpret the kinetics of channel opening and closing according to the following scheme

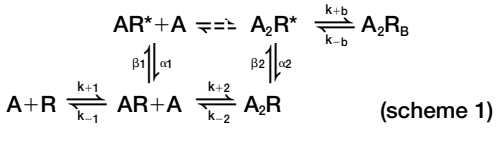

(scheme 1)

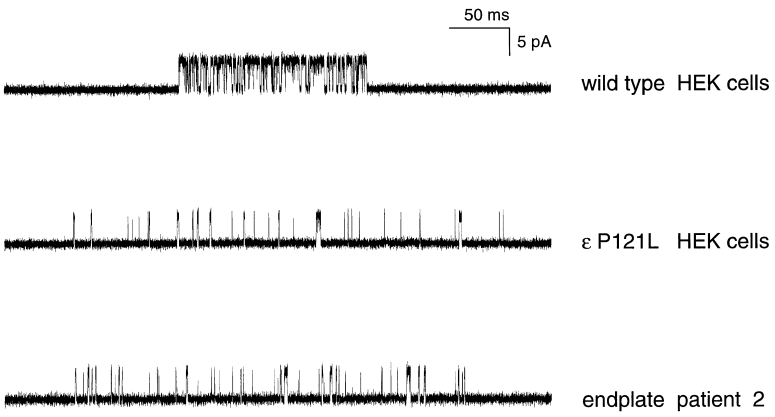

Figure 6. Comparison of Single Channel Currents from EP and Engineered ϵP121L AChRs

Clusters of single-channel currents elicited by high concentrations of ACh are shown, with openings upward deflections. Wild type corresponds to the engineered adult human AChR ($\alpha_2\beta\epsilon\delta$) in the presence of 50 μM ACh, ϵP121L to the engineered mutant AChR ($\alpha_2\beta\delta\epsilon$P121L) in the presence of 200 μM ACh, and EP to the AChR at an EP from patient 2 in the presence of 50 μM ACh.

where two agonists A bind to the resting state of the receptor R with association rates k_{+1} and k_{+2} and dissociate with rates k_{-1} and k_{-2}. Receptors occupied by one agonist open with rate β_1 and close with rate α_1, while receptors occupied by two agonists open with rate β_2 and close with rate α_2. At high concentrations, ACh blocks the open channel with forward rate k_{+b}, and unblocks with rate k_{-b}. To estimate each rate constant, dwell times predicted by scheme 1 were fit by maximum likelihood to all of the data simultaneously; for each type of AChR, this included open and closed durations obtained for the entire range of ACh concentrations. The results of the fit, shown as smooth curves superimposed on the open and closed duration histograms, adequately describe the kinetics of both wild-type and ϵ121L AChR (Figure 7).

The fitting analysis establishes that ϵP121L markedly affects the kinetics of channel gating. Once doubly occupied, the wild-type AChR opens rapidly and efficiently, whereas the ϵP121L AChR opens with profound latency and reduced efficiency (Figure 7); both opening rate and open channel equilibrium constant are reduced 300- to 400-fold (Table 3). Opening of the singly occupied AChR, although slower than that of the doubly occupied AChR, is slowed about 14-fold by ϵP121L (Table 3). The effect of ϵP121L on gating is almost entirely confined to the channel opening step, with little effect on channel closing (Table 3).

Rates of association and dissociation of ACh are affected to a lesser extent by ϵP121L. For the human wild-type AChR, the rate of association is rapid and near the limit of diffusion, as described for other species (Sine et al., 1990; Zhang et al., 1995). Although slowed about 5-fold by ϵP121L, the rate of association is still fast enough to support rapid activation at the high concentrations of ACh present at the synapse (Table 3). For the human wild-type AChR, the rate of dissociation of ACh from the second site is rapid, but that from the first site is slower (Table 3). The presence of ϵP121L slows dissociation approximately 3-fold from the second site, and has no detectable effect on dissociation from the first site. The resulting association and dissociation rate constants indicate that ϵP121L causes little change in the affinity of ACh for the resting state of the AChR (Table 3). Error estimates for association and dissociation rate constants were greater for the mutant than for the wild-type AChR; presumably this resulted from inability to analyze data for the mutant AChR at ACh concentrations below 30 μM owing to lack of clustering (see Experimental Procedures). Also, well-defined rate constants for both sites could only be obtained by assuming equivalent binding sites for ϵP121L. Relaxing the constraint of equivalent sites yielded similar parameters for the second binding step, but undefined parameters for the first step (data not shown). Nevertheless the kinetic analysis of ϵP121L reveals relatively small changes in rate constants governing ACh binding to the resting state, but profound changes in channel gating.

Binding of ACh to the open state of the AChR can be envisioned by connecting the singly and doubly occupied open states in scheme 1 (dashed lines). Applying the principle of microscopic reversibility to the resulting closed cycle, we obtain $\theta_1 K_2 = \theta_2 K_2^*$, where θ_1 and θ_2 are the opening equilibrium constants of the singly and doubly occupied states, and K_2 and K_2^* are the dissociation constants for ACh binding to the resting and open states. Given θ_1, θ_2, and K_2 estimated from kinetic analysis, we calculate K_2^* for the wild-type AChR to be 35 nM, whereas that for the ϵP121L mutant is 1450 nM (Table 3). Thus, in addition to affecting channel gating, ϵP121L reduces the affinity of ACh for the open channel.

ϵP121L Reduces the Affinity of the AChR for ACh

Owing to its proximity to residues that contribute to binding of the competitive antagonists *d*-tubocurarine and conotoxin M1 (residues 111 and 117; Figure 4; Sine, 1993; Sine et al., 1995), ϵP121L might affect ACh affinity by perturbing the contribution of the ϵ subunit to the binding site. Therefore, we sought direct evidence for an effect of ϵP121L on the binding site.

To examine the binding site in its simplest form, we coexpressed α and either wild-type or mutant ϵ subunits and measured ACh binding to HEK cells permeabilized with saponin. Oligomers of α and ϵP121L subunits bind ACh with markedly reduced affinity (Figure 8A). Thus, the interaction of ϵP121L with the α subunit is sufficient to reduce affinity for ACh; neither a fully assembled pentamer nor the presence of β and δ subunits is required.

We then examined equilibrium binding of ACh to cells transfected with either wild-type or mutant ϵ subunits plus complementary α, β, and δ subunits. The fully assembled human AChR binds ACh cooperatively and with

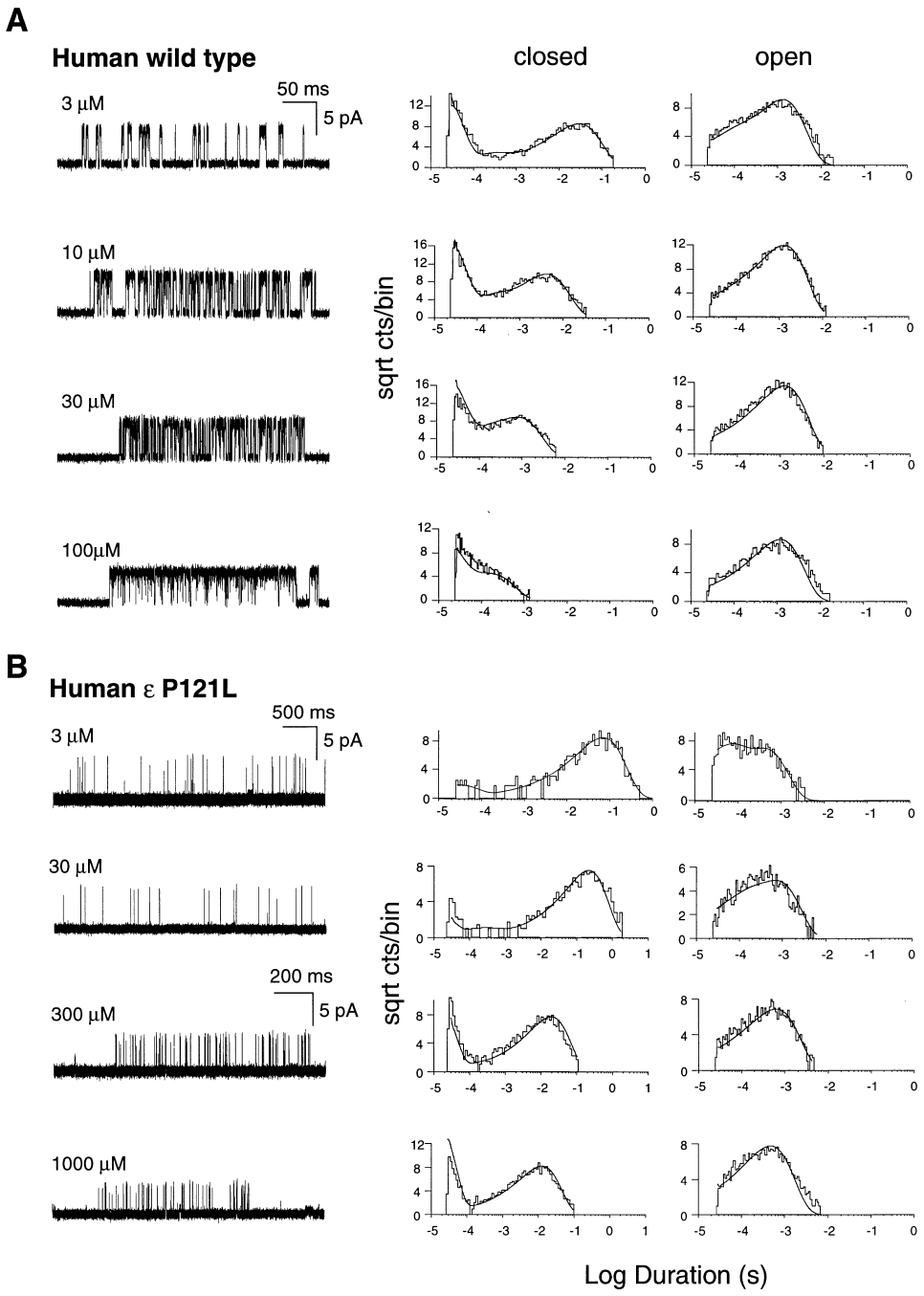

Figure 7. Kinetics of Activation of Human Wild-Type and ϵP121L AChRs

(A) Individual clusters of single-channel currents recorded from HEK cells expressing human wild-type AChR ($\alpha_2\beta\epsilon\delta$) at the indicated ACh concentrations at a bandwidth of 9 kHz (left column). Histograms of closed and open durations for each ACh concentration are shown with the results of the fit to scheme 1 superimposed (center and right columns). The fitted rate constants are given in Table 3.

(B) Individual clusters of single-channel currents recorded from HEK cells expressing human mutant AChR ($\alpha_2\beta\delta\epsilon$P121L) at the indicated ACh concentrations (left column). For the recording obtained at 3 μM ACh, openings do not cluster, so a representative segment of the recording is shown. Histograms of closed and open durations for each ACh concentration are shown with the results of the fit to scheme 1 superimposed (center and right columns). The fitted rate constants are given in Table 3. For the recording obtained at 3 μM ACh, the lack of clustering prevented identification of a series of events corresponding to a single channel, so scheme 1 cannot be applied to these data. Instead, fits to the sum of exponentials are presented (smooth curves) with the following time constants and relative areas: closed, τ_0 = 34 μs, a_0 = 0.04, τ_1 = 69 ms, a_1 = 0.96; open, τ_0 = 39 μs, a_0 = 0.49, τ_1 = 0.4 ms, a_1 = 0.51; total events, 1058.

Table 3. Kinetic Parameters for Activation of Human Wild-Type and ϵP121L AChRs Expressed in HEK cells

Wild Type	k_{+1}	k_{-1}	$K_1/\mu M$	k_{+2}	k_{-2}	$K_2/\mu M$	β_1	α_1	θ_1	β_2	α_2	θ_2	K_2^*/nM	k_{+b}	k_{-b}	K_B/mM
Scheme 1	151 (± 8)	2,880 (± 224)	19	106 (± 3)	15,200 (± 244)	143	58.2 (± 5.2)	10,400 (± 1,380)	5.6E-3	50,900 (± 1,340)	2,160 (± 64)	23	35	48.3 (± 13.8)	155,000 (± 10,700)	3.2
Scheme 2	102 (± 5)	2,420 (± 183)	23	109 (± 4.31)	12,700 (± 597)	116	59.9 (± 3.8)	10,300 (± 1,000)	5.8E-3	50,600 (± 3,350)	2,140 (± 296)	24	28	48.6 (± 13.7)	155,000 (± 9,840)	3.2
ϵ P121L	k_{+1}	k_{-1}	$K_1/\mu M$	k_{+2}	k_{-2}	$K_2/\mu M$	β_1	α_1	θ_1	β_2	α_2	θ_2	K_2^*/nM	k_{+b}	k_{-b}	K_B/mM
Scheme 1	38.7 (± 8.6)	2,460 (± 545)	63	19.4 (± 4.3)	4,930 (± 1,090)	255	4.1 (± 0.58)	8,910 (± 1,310)	4.6E-4	115 (± 4)	1,410 (± 20)	0.081	1450	9.02 (± 1.53)	98,500 (± 6,530)	10.9

Rate constants are as defined in scheme 1 (see text), in units of $\mu M^{-1}\ s^{-1}$ for association rate constants, and s^{-1} for all others. Values are results of a global fit of scheme 1 to data obtained over a range of ACh concentrations, with standard errors in parenthesis (see Experimental Procedures). Channel open equilibrium constants, θ, are ratios of the corresponding opening to closing rate constants, β/α. K_2^* is the dissociation constant for ACh binding to the opening state calculated according to the principle of microscopic reversibility (see text). Scheme 2 is a modification of scheme 1 to allow nonsequential binding of ACh; fitting according to scheme 2 yielded well-defined rate constants only for the wild-type AChR. For the ϵP121L AChR, equivalent binding sites were assumed (see text), so the rate constants include the following statistical factors: $k_{+1} = 2k_{+2}$, $2k_{-1} = k_{-2}$.

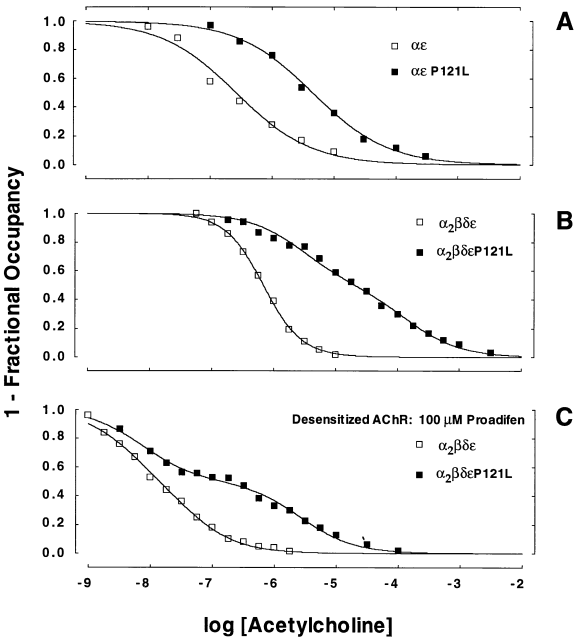

Figure 8. ϵP121L Decreases Acetylcholine-Binding Affinity

(A) Acetylcholine binding to saponin-permeabilized cells transfected with the indicated pairs of subunits determined by competition against the initial rate of ^{125}I-α-bgt binding. The curves are fits to the Hill equation (Equation 1) with the following parameters: αϵ, $K_{ov} = 2.45 \times 10^{-7}$, n = 0.7; αϵP121L, $K_{ov} = 4.3 \times 10^{-6}$, n = 0.7.

(B) Acetylcholine binding to intact cells transfected with the indicated four subunits. For wild type ($\alpha_2\beta\epsilon\delta$) the curve is a fit to Equation 1 with $K_{ov} = 6.85 \times 10^{-7}$, and n = 1.4. For mutant ($\alpha_2\beta\delta\epsilon$P121L), the curve is a two-site fit (Equation 2) with $K_A = 2.9 \times 10^{-6}$, $K_B = 1.45 \times 10^{-4}$, and $fract_A = 0.5$.

(C) Acetylcholine binding to intact cells transfected with the indicated four subunits in the presence of 100 μM proadifen. The curves are fits to Equation 2 with the following parameters: wild type ($\alpha_2\beta\delta\epsilon$), $K_A = 4.8 \times 10^{-9}$, $K_B = 4.1 \times 10^{-8}$, $fract_A = 0.5$; mutant ($\alpha_2\beta\delta\epsilon$P121L), $K_A = 7.5 \times 10^{-9}$, $K_B = 2.7 \times 10^{-6}$, $fract_A = 0.5$.

micromolar affinity, as described for the adult mouse AChR (Sine et al., 1995). However, in the presence of ϵP121L, the ACh binding profile is markedly broadened, and is described as the sum of two components, one with close to normal affinity and the other with markedly reduced affinity (Figure 8B). Thus, in the fully assembled pentamer, ϵP121L appears to reduce the affinity of one of the two binding sites for ACh.

Binding of ACh at equilibrium includes contributions of resting, open channel and desensitized states of AChR, each of which binds ACh with different affinity (for review, see Changeux, 1990). To examine binding to a single state, we measured ACh binding in the presence of a high concentration of the local anesthetic proadifen, which converts the AChR to the desensitized state (Weiland et al., 1977; Sine and Taylor, 1982). In the presence of 100 μM proadifen, ACh binds to the wild-type AChR with high affinity and with similar affinity for the two binding sites (Figure 8C). By contrast, the ϵP121L AChR exhibits a biphasic profile with one component of normal affinity and the other with markedly reduced affinity. Thus, when binding to the desensitized state is measured, the effect of ϵP121L is seen to be restricted to one of the two binding sites where the affinity for ACh is reduced 65-fold.

Discussion

Our initial report of patient 1 postulated that the defect of neuromuscular transmission was caused by an abnormal interaction of ACh with its receptor (Uchitel et al., 1993). This hypothesis was based on the reduced MEPP amplitude without EP AChR deficiency, the normal size of the synaptic vesicles, and the abnormal power spectrum of the ACh induced current noise. Patch-clamp studies of EP AChRs in patient 2, who also has small MEPPs without EP AChR deficiency, discovery of the pathogenic mutations in both patients, and analysis of the properties of the mutant AChRs in HEK cells confirm the postulated disease mechanism.

Phenotype Effects of the Mutations

All three mutations are recessive, as each mutation is present in an unaffected relative. ϵP121L, shared by both patients, is near residues that affect ligand-binding affinity (Sine, 1993; Sine et al., 1995a) and AChRs harboring this mutation are expressed in normal amounts in HEK cells. Expression studies also suggest that ϵG-8R, the signal peptide mutation found in patient 1, and ϵS143L, the glycosylation consensus site mutation in patient 2, result in markedly reduced protein expression at the EP, or may even act as null mutations. These findings predict that the clinical phenotype in both patients is defined by the consequences of ϵP121L mutation.

Structural Interpretation

Mutagenesis, affinity labeling and expression studies have established that the two ACh-binding sites of the adult AChR are formed by pairs of subunits, αδ and αϵ. The δ and ϵ subunits are required for maturation of the binding sites to produce high affinity for small ligands and selective binding of agonists and antagonists (Blount and Merlie, 1989; Sine and Claudio, 1991). Studies of the site-selective ligands, dimethyl-*d*-tubocurarine (DMT) and conotoxin M1, identified three regions of the extracellular domain of the non-α subunits that contribute to the binding site: N-terminal, predisulfide and postdisulfide regions (Sine 1993; Sine et al., 1995). The predisulfide region (containing residues 111 and 117 equivalent to those in the γ and δ subunits that contribute to selective binding of DMT and conotoxin M1) contains P121 and is likely to be affected by the mutation (Figure 4). Although the predisulfide region is recognized to contribute to antagonist binding, the present results firmly establish its importance for agonist binding as well. Both mutagenesis (Fu and Sine, 1994) and photolabeling (Chiara and Cohen, 1992) studies suggest that the predisulfide region is in close proximity to the binding site. Owing to conformational restriction by its imino ring, proline at position 121 may orient the predisulfide region in a conformation essential for stabilizing ACh in the binding site.

State-Specific Decrease in ACh Affinity by ϵP121L

The affinity of the AChR for ACh depends on its functional state (for review, see Changeux, 1990). ACh binds to the resting state at concentrations in the range of

10^{-4} M, whereas it binds to the open channel and desensitized states in the range of 10^{-8} M (Table 3; Figure 8C). The resting state predominates in the absence of ACh, with its relatively low affinity still sufficient to bind ACh at concentrations of several hundred micromolar present during synaptic activity. However, in the presence of ACh, high affinity binding to the open channel and desensitized states draws the AChR out of the stable resting state, allowing these functional states to accumulate in significant amounts (Jackson, 1989). Without the stabilization provided by high affinity binding of ACh, the open and desensitized states would occur with low probability, as we observe for the εP121L AChR.

The decrease in ACh-binding affinity by εP121L is evident in the simplest form of the binding site, that of the αε dimer, although the relationship of the dimer to a particular functional state is not known. Our kinetic measurements on the fully assembled pentamer show little change in affinity of the resting state for ACh, but calculations based on microscopic reversibility suggest a 40-fold decrease in the affinity for the open-channel state. Thus, the low probability of opening of the εP121L AChR owes to impaired stabilization of the open state by ACh. By measuring binding to the high affinity desensitized state, we find a similar 65-fold decrease in affinity of one of the two binding sites for ACh. Again, the reduced extent of desensitization of the εP121L AChR owes to inadequate stabilization of the desensitized state by ACh. Our overall results suggest that εP121L decreases the affinity of one of the two binding sites for ACh, presumably αε, and that the decrease is selective for functional states, open and desensitized.

Implications for AChR Activation

In addition to affecting the affinity of functional states for ACh, εP121L markedly slows the rate of channel opening (β_2, Table 3). The rate of channel opening is a measure of the height of the free energy barrier in the pathway toward opening, whereas the affinity for ACh is a measure of the net change in free energy due to association and dissociation of ACh. We find similar changes in free energy of the two parameters: εP121L increases free energy required for channel opening by 3.6 kcal/mole, while it decreases free energy of ACh binding by 2.2 and 2.5 kcal/mole for the open and desensitized states, respectively. The dual effect of εP121L on opening rate and ACh affinity suggests that the site of ACh binding is closely coupled to the site that triggers channel opening. Studies of the site-directed mutation αY190F also reveal a decreased rate of channel opening and a decrease in ACh binding affinity (Chen et al., 1995). Thus, favorable contacts between ACh and its binding site appear to be an essential requirement for forming the transition state for channel opening.

Properties of EP AChRs

Patch-clamp studies in patient 2 enabled us to compare the properties of mutant AChRs at the EP with those of engineered mutant AChRs expressed in HEK cells. In patient 2, the 60 pS EP channel events comprise a major and minor component (see arrows, Figure 2). The minor component has open interval and burst durations that resemble those predominating at control EPs (Figure 2; Table 2). The origin of these channel events cannot be determined with certainty but they likely reflect a low level of expression of the ε allele harboring S143L. We attribute the major component of EP channel events to AChRs containing εP121L because the engineered εP121L AChR shows robust expression and is kinetically similar to the EP AChR. The kinetic similarities include infrequent channel events and diminished channel reopenings during ACh occupancy caused by a decreased channel opening rate, and resistance to clustering at high concentrations of ACh that suggests resistance to desensitization. In addition, the mean burst duration at the EPs of patient 2 (0.45 ms; τ_1 in Table 2) is shorter than normal (2.99 ms; τ_2 in Table 2); presumably this is due to the reduced opening rate in the patient and thus fewer reopenings during ACh occupancy. This difference in burst duration is paralleled in the expression system where the mean burst duration for the mutant (0.7 ms, obtained from $1/\alpha_2$; Table 3) is shorter than that for wild type (2.0 ms, obtained from $([1 + \beta_2/k_{-2}]/\alpha_2$; Table 3). Quantitative differences between AChRs at EPs of patient 2 and in the expression system may owe to differences in recording conditions (see Experimental Procedures).

Effects of the εP121L Mutation on Neuromuscular Transmission

The εP121L mutation affects the safety margin of neuromuscular transmission primarily by reducing the synaptic response to ACh quanta. Following release of ACh at the synapse, both binding sites of the mutant AChR are likely to be doubly occupied because the concentration of ACh is high and the decrease in affinity of the resting state for ACh is only about 2-fold. However, the probability that a given occupancy will result in channel opening depends on the rate of channel opening relative to the rate of ACh dissociation, or the ratio β_2/k_{-2}. Our kinetic analysis demonstrates a dramatic slowing of the channel opening rate but little change in the rate of ACh dissociation. Thus, β_2/k_{-2} is approximately 0.023 for the εP121L mutant, whereas it is 3.3 for the normal AChR (Table 3). Thus, the markedly decreased MEPP amplitude is readily explained by a diminished number of receptors being activated. Furthermore, the duration of the synaptic current is curtailed by the shorter than normal burst open duration.

The properties of the εP121L mutation also have therapeutic implications. They predict a favorable response to 3,4-diaminopyridine, which increases the number of ACh quanta released by nerve impulse (Thomsen and Wilson, 1983) and thereby the number of postsynaptic sites activated by ACh. Indeed, patient 1 has improved significantly with this medication. Anticholinesterase drugs, which prolong the duration of the synaptic response (Katz and Miledi, 1973), will also be beneficial, and the resistance of the mutant AChR to desensitization predicts that relatively high doses of these drugs can be employed in clinical practice.

Comparison with Other Congenital Myasthenic Syndromes

Clinical criteria, such as weakness increased by exertion and a decremental response of the evoked compound

muscle action potential, do not distinguish the present syndrome from other CMS. However, the εP121L mutation is unique in that it leaves no anatomic footprint at the EP. For example, the slow channel CMS (SCCMS) causes an EP myopathy by cationic overloading, and CMS stemming from simple AChR deficiency show a diminished density of AChR on the junctional folds (Engel, 1994b). It is also noteworthy that SCCMS mutations prolong the burst open duration (Ohno et al., 1995a and 1995b; Sine et al., 1995b) whereas εP121L curtails it. Also, the SCCMS caused by the αG153S mutation is associated with enhanced agonist binding affinity, increased channel reopenings during ACh occupancy, and increased desensitization of the mutant AChR by ACh (Sine et al., 1995b). By contrast, the εP121L mutation results in diminished agonist binding affinity, reduced channel reopenings during ACh occupancy, and decreased desensitization of the mutant AChR by ACh. For these reasons, we propose the descriptive term of low- affinity fast-channel syndrome for the present disorder. Finally, our study implies that mutations diminishing agonist binding affinity may also occur in central ligand-gated channels and should spur the search for such mutations in neurologic and psychiatric disorders of unknown etiology.

Experimental Procedures

Muscle Specimens

Intercostal muscle specimens were obtained intact from origin to insertion from the patients and from control subjects without muscle disease undergoing thoracic surgery. All human studies were in accord with the guidelines of the Institutional Review Board of the Mayo Clinic.

Electron Microscopy

An intercostal muscle specimen was used. EPs were localized and analyzed morphometrically by established methods (Engel, 1994a). Peroxidase-labeled α-bgt was used for the ultrastructural localization of AChR (Engel et al., 1977).

Intracellular Microelectrode Studies

All studies were done at 22°C ± 0.5°C. MEPPs and EPPs were recorded as previously described (Engel et al., 1993). The number of transmitter quanta released by nerve impulse (*m*) was determined at 1 Hz stimulation by the variance method with correction for a resting membrane potential of −80 mV, nonlinear summation, and non-Poisson release (Elmqvist and Quastel, 1965; Martin, 1966; Lang et al., 1983). Due to their abnormally small amplitude, MEPPs could not be recorded directly. Therefore, the MEPP amplitude for a given EP was derived from the ratio of *A*/*m*, where *A* is the mean EPP amplitude recorded from uncurarized muscle (Elmqvist and Quastel, 1965). The value so obtained was further corrected for the smaller than adult size of the muscle fibers of the patient (29 μm versus 50 μm) (Katz and Thesleff, 1957).

Counts of AChR per EP in Patient 2

The number of AChRs per EP was measured with ^{125}I-labeled α-bgt, as previously described (Engel et al., 1993).

Patch-Clamp Recordings from EP AChRs

These were performed in the cell-attached mode by a slight modification of the previously described method (Milone et al., 1994). The bath and pipette solutions contained 135 mM NaCl, 5 mM KCl, 2 mM $CaCl_2$, 1 mM $MgCl_2$, 15 mM $NaHCO_3$, 1.3 mM Na_2HPO_4, 11.1 mM dextrose (pH 7.2) with the pipette solution containing specified concentrations of ACh. Owing to trauma induced by microdissection of single-muscle fibers, we obtained a null resting potential. This was confirmed by the absence of detectable channel events with 0 mV applied to the pipette. For all patches, the membrane potential was set to −80 mV; when possible, recordings were also obtained at −40, −120, and −160 mV. Channel currents were recorded at 50 kHz using the Axopatch 200A amplifier (Axon Instruments), digitized at 100 kHz, stored on hard disk, and analyzed using the program MacTac (Instrutech) at a final bandwidth of 12 kHz. Burst durations were determined by grouping openings separated by a specified closed time that misclassifies equal proportions of long closed times within bursts and short closed intervals between bursts (Colquhoun and Sakmann, 1985). Dwell time histograms were plotted on logarithmic abscissa and fitted to the sum of exponentials by maximum likelihood (Sigworth and Sine, 1987).

mRNA and DNA Samples

mRNA was obtained using the Micro-FastTrack mRNA isolation kit (Invitrogen). First-strand cDNA was prepared from mRNA by using random hexamer primers with the cDNA Cycle kit (Invitrogen) and by following the instructions of the manufacturer. Genomic DNA was isolated from proteinase/SDS digest of blood or muscle by phenol-chloroform extraction followed by ethanol precipitation (Sambrook et al., 1989).

PCR Procedures

PCR primers for SSCP analysis and sequencing were prepared as previously described (Ohno et al., 1995a). The typical PCR reaction mixture included 60 mM Tris-HCl (pH 8.5), 15 mM $(NH_4)_2SO_4$, 1.5 mM $MgCl_2$, 0.25 mM each dNTP, 0.8 μM each primer, with 100 ng of DNA and 1.25 U of *Taq* DNA polymerase (Boehringer Mannheim) in 50 μl. The typical cycling protocol consisted of denaturation at 94°C for 2 min, 35 cycles of 94°C for 30 s, 55°C for 30 s, 72°C for 3 min, and final extension at 72°C for 7 min.

We used allele-specific PCR to search for the εG-8R mutation, detected in ε-exon 1 in patient 1, and for the εS143L mutation, detected in ε-exon 5 in patient 2, in the patients' relatives and normal controls. For the εG-8R mutation, the respective wild-type and mutant sense primers were 5′-GGGTCCTGCTCCTCTaGG-3′ and 5′-GGGTCCTGCTCCTCTaGA-3′. Mismatched nucleotide 'a' was introduced three nucleotides upstream to the 3′ end of the primer to avoid misannealing of the primer to the opposite allele. The antisense primer was 5′-GAAGTGGGATTTTTGGCTTA-3′ in ε subunit gene intron 2. The expected PCR product had 467 bp. The PCR procedure was optimized by adding 2.0 mM $MgCl_2$ and 10% dimethyl sulfoxide.

For the εS143L mutation, the respective wild-type and mutant sense primers were 5′-TTCGATTGGCAGAACTGaTC-3′ and 5′-TTCGATTGGCAGAACTGaTT-3′, 'a' representing a deliberately mismatched nucleotide. The antisense primer was 5′-GAAGCGGGTTTTTCTGAG-3′ in ε subunit gene intron 6. The expected PCR product had 473 bp. The standard PCR procedure was employed.

Exon Scanning by SSCP Analysis

The "cold" SSCP procedure was employed (Hongyo et al., 1993) with ca. 500 ng of PCR-amplified DNA. Denatured SSCP samples were loaded on 4%–20% gradient polyacrylamide gel, electrophoresed at 12°C, stained with ethidium bromide, and examined under ultraviolet light.

Sequence Analysis

PCR-amplified fragments of genomic DNA or cDNA were purified by Wizard PCR Preps (Promega). Plasmids were purified by QIAwell 8 Plus Plasmid kit (Qiagen). DNA fragments and plasmids were sequenced with an Applied Biosystems model 373A DNA sequencer using fluorescently labeled dideoxy terminators.

Restriction Enzyme Analysis

A 211 bp fragment of genomic DNA spanning the εP121L mutation was amplified with primers 5′-TGCAAAAAGCTCGGTTTC-3′ and 5′-GGCCTCGGAGTAGCTCTT-3′. The PCR product (25 μl) was purified by ethanol precipitation. Restriction enzyme digestion was carried out by incubating the purified PCR product, 2 μl of 10 × reaction buffer and 5 U MspI (Boehringer-Mannheim), in a volume of 20 μl at 37°C for 2 hr. The products were size-fractionated on 4% agarose gel containing ethidium bromide.

Cloning of Human β- and ε-Subunit cDNAs

cDNA for the normal human β subunit was cloned from a nested RT-PCR product amplified from normal muscle. The first primers for amplification were 5′-GGCGAGCCGCCAGCGTATGA-3′ (nucleotides −85 through −66) and 5′-AAGAGGCAGAGAAGGATAGG-3′ (nucleotides 1503 through 1522); the nested primers were 5′-cggccg gaattcATGACCCCAGGGGCTCTG-3′ (nucleotides −69 through −52) and 5′-cggccggaattcGGCTTGACAGTATCACCAAACT-3′ (nucleotides 1482 through 1503), the artificial lower case sequences serving to introduce EcoRI sites into the PCR product. The nested PCR product spanned nucleotides -69 through 1504, whereas the coding region of the β subunit extends from −69 to 1434. The nested PCR product was precipitated with ethanol, digested with EcoRI, gel-purified, and then ligated in pBluescript II SK(−) (Stratagene) using a DNA Ligation Kit (PanVera). Since the β subunit cDNA cloned in this manner failed to express in HEK cells, we introduced the Kozak sequence for the β subunit gene 5′ to nucleotide −69 by the megaprimer method (Kozak, 1987; Uppender et al., 1995), using cloned *Pfu* DNA polymerase (Stratagene). For the first round of PCR, the template was the cloned β subunit cDNA; the primers consisted of the 5′-GGAAACAGCTATGACCATG-3′ generic primer for M13 and 5′-CAGCAGAGCCCCTGGGGTCATAGCCTGGCGgaattcctgcagccc gggggatc-3′, where the underlined nucleotides represent the Kozak sequence of the β subunit gene and the lower case sequence is part of the pBluescript II SK(−) multiple cloning site. The amplified 156-bp fragment contained part of the plasmid multiple cloning site, the Kozak sequence, and the first 21 nucleotides of the β subunit gene coding region. For the second round of PCR, the megaprimer was 3 ng of the purified product of the first run of PCR and the template consisted of the cloned β subunit excised from the plasmid with EcoRI. The second round of PCR consisted of 10 cycles performed with the megaprimer as the only primer and 25 additional cycles in the additional presence of 40 pmoles each of the M13 generic primer and 5′-cggccggaattcGGCTTGACAGTATCACCAA ACT-3′ (nucleotides 1482 through 1503), the artificial lower case sequence serving to introduce the EcoRI sites into the PCR product. The second PCR product was cut by EcoRI, ligated into pBluescript II SK(−), and then transferred to the pRBG4 expression vector (Lee et al., 1991).

We sequenced our β clone and compared it with the reference sequence of the human β subunit gene (GenBank accession number X14830, modified from Beeson et al., 1989) and with cDNA and DNA of our human controls. Comparison with the reference sequence revealed 3 discordant nucleotides in the coding region (G instead C at position −27, indicating an alanine instead of a proline at codon −9; G instead A at position 26, indicating a glycine instead of a glutamate at codon 9; and T instead of A at position 560 indicating an isoleucine instead of an asparagine at codon 187), as well as 3 discordant nucleotides in the 3′ untranslated region (insertion of a C at position 1456, and deletion of GA at positions 1478–1479). Direct sequencing of both cDNA and genomic DNA from 18–20 human controls indicated nucleotides identical to those in our clone and no polymorphisms at positions −27, 560, 1456, 1478, and 1479. However, 26G in our β subunit clone proved to be a common polymorphism, being detected in 17 out of 60 alleles by BsaJI restriction analysis.

The first PCR primers for amplification of the ε subunit were 5′-CACGCAGCAGGATGGCAAGG-3′ (nucleotides −71 through −52) and 5′-TGGAAGACTGGCACCTGAGA-3′ (nucleotides 1631 through 1650); the nested PCR primers were 5′-cggccggaattcATGGCAA GGGCTCCGCTT-3′ (nucleotides −60 through −43) and 5′-cggccg gaattcCAGGGGGAAGGGATCATAAT-3′ (nucleotides 1499 through 1518), the lower case sequences comprising the EcoRI site. The PCR reaction mixture contained 1.25 units of cloned *Pfu* DNA polymerase, 10% dimethyl sulfoxide, and Pfu buffer (Stratagene) in 50 μl. The first PCR was carried out by denaturation at 94°C for 2 min followed by 25 cycles of 94°C for 30 s, 55°C for 30 s, and 72°C for 90 s. The nested PCR was carried out under identical conditions but the denaturation step was followed by 30 cycles of amplification. The nested PCR product spanned nucleotides −60 through 1518 of the ε subunit gene, whereas the coding region of the ε subunit extends from nucleotides −60 through 1419. The second PCR product was cut by EcoRI, ligated into pBluescript II SK(−), and then transferred to the pRBG4 expression vector (Lee et al., 1991).

Sequencing of our ε clone revealed no mutation or polymorphism when compared with our controls and to the reference sequence of human ε subunit gene (GenBank accession number X66403, modified from Beeson et al., 1993). Therefore, we assume that our clone has the consensus sequence.

Construction of Human Wild-Type and Mutant AChR cDNAs and Expression in 293 HEK Cells

Human α and δ subunit cDNAs were provided by Dr. Jon Lindstrom (Schoepfer et al., 1988; Luther et al., 1989). The β and ε subunit cDNAs were cloned from normal human skeletal muscle as described above. All four cDNAs were subcloned into the CMV-based expression vector pRBG4 (Lee et al. 1991) for expression in 293 HEK cells. The εP121L and εS143L mutations were constructed by bridging restriction sites with synthetic double stranded oligonucleotide harboring the mutations. For εP121L, a 64 bp oligonucleotide bridged from an AccI to a BstEII site, whereas for εS143L, a 105 bp oligonucleotide bridged from an FspI to an AccI site. The presence of each mutation and the absence of unwanted mutations was confirmed by dideoxy sequencing. The εG-8R mutation was constructed by overlap PCR; the final amplified fragment was ligated between a PstI site in the poly linker of pRBG4 and a Bsu36I site within the ε cDNA, and was sequenced in its entirety. Human embryonic kidney fibroblast cells (293 HEK) were transfected with mutant or wild-type AChR subunit cDNAs using calcium phosphate precipitation as described (Bouzat et al., 1994).

Patch-Clamp Recordings from AChRs Expressed in HEK Cells

Recordings were obtained in the cell-attached configuration (Hamill et al., 1981) at a membrane potential of −70 mV and a temperature of 22°C (Bouzat et al., 1994). The bath and pipette solutions contained 142 mM KCl, 5.4 mM NaCl, 1.8 mM $CaCl_2$, 1.7 mM $MgCl_2$, 10 mM HEPES (pH 7.4). Single channel currents were recorded using an Axopatch 200A at a bandwidth of 50 kHz, digitized with a PCM adapter at 94 kHz (VR-10B, Instrutech Corporation), transferred to a Macintosh computer using the program Acquire (Instrutech Corporation), and detected by the half-amplitude threshold criterion using the program MacTac (Instrutech Corporation) at a final bandwidth of 9 kHz. Open and closed duration histograms were constructed using a logarithmic abscissa and square root ordinate (Sigworth and Sine, 1987), and fitted to the sum of exponentials by maximum likelihood. For kinetic analysis according to scheme 1, clusters of openings corresponding to a single channel were identified as a series of closely spaced events preceded and followed by closed intervals greater than a specified duration; this duration was taken as the point of intersection of the predominant closed time component in the histogram and the succeeding closed time component. Clusters were then examined for homogeneity in terms of open probability and mean open duration; clusters within two standard deviations of the mean for each parameter were accepted for further analysis. For wild type, greater than 90% of clusters were accepted, while for the εP121L AChR all clusters were accepted. Finally, clusters with greater than 10 events for wild type and greater than two events for εP121L were accepted. Once identified, the clusters of open and closed intervals were entered into a table, transferred to an IBM RS6000 computer, and analyzed according to scheme 1 using an interval-based maximum likelihood method that incorporated corrections for missed events (Qin et al., 1996). Single channel dwell times, obtained from single patches at several concentrations of ACh, were fitted simultaneously. For wild-type AChR, concentrations of ACh used for analysis and events analyzed were: 3 μM (2576 events, 45 clusters), 5 μM (3401 events, 84 clusters), 10 μM (4133 events, 37 clusters), 30 μM (4051 events, 42 clusters), 50 μM (3516 events, 102 clusters), and 100 μM (2091 events, 37 clusters). For the εP121L mutant, concentrations used for analysis and events analyzed were: 30 μM (960 events, 34 clusters), 100 μM (1071 events, 23 clusters), 200 μM (2050 events, 15 clusters), 300 μM (1731 events, 23 clusters), and 1000 μM (1821 events, 17 clusters). A uniform filter bandwidth of 9 kHz and a dead time of 25 μs were imposed for all recordings. After fitting, error estimates for each parameter were determined as described (Qin et al., 1996). Open and closed duration histograms were calculated from the fitted rate constants and superimposed on the experimental dwell time histograms.

ACh Binding Measurements

Three days after transfection, intact HEK cells were harvested by gentle agitation in phosphate buffered saline (PBS) plus 5 mM EDTA. We added 1 μM esterase inhibitor diisopropylphosphofluoridate to the PBS/EDTA solution, and cells were incubated for 15 min. Cells were briefly centrifuged, resuspended in high potassium Ringer's solution, and divided into aliquots for measurements of ACh binding. High potassium Ringer's solution contains 140 mM KCl, 5.4 mM NaCl, 1.8 mM $CaCl_2$, 1.7 mM $MgCl_2$, 25 mM HEPES, 30 mg/liter bovine serum albumin, adjusted to pH 7.4 with 10 mM–11 mM NaOH. Specified concentrations of ACh were added 30 min prior to addition of ^{125}I-labeled-α-bgt (5 nM), which was allowed to bind for 30 min to occupy approximately half of the surface receptors. Binding of ^{125}I-α-bgt was stopped by adding potassium Ringer's solution containing 300 μM *d*-tubocurarine, followed by filtration using a cell harvester (Brandel Incorporated). Radioactivity retained by the glass fiber filters (Whatman GF-B, 1 μm cutoff) was measured with a gamma counter. Binding properties of αϵ dimers were determined in cells permeabilized with saponin by modification of the method of Blount and Merlie (1991). After removing the growth medium, cells were incubated for 5 min in PBS/EDTA plus 0.1% BSA and 0.5% saponin. Following addition of high potassium Ringer's solution, cells were briefly centrifuged, resuspended in high potassium Ringer's solution, and divided into aliquots for ACh-binding measurements. The total number of binding sites was determined by incubating cells for 1 hr in the presence of 5 nM ^{125}I-labeled-α-bgt. Nonspecific binding was determined in the presence of 300 μM *d*-tubocurarine. The initial rate of ^{125}I-α-bgt binding was determined to yield fractional occupancy of sites by ACh (Sine and Taylor, 1979). Competition measurements were analyzed according to either the monophasic Hill equation (Equation 1) or the sum of two distinct binding sites (Equation 2):

$$1\text{-}Y = 1/(1 + ([ACh]/K_{ov})^n) \quad (1)$$

$$1\text{-}Y = \text{fract}_A(1/(1 + [ACh]/K_A) + (1\text{-fract}_A)(1/(1 + [ACh]/K_B) \quad (2)$$

where Y is fractional occupancy by ACh, K_{ov} is an overall dissociation constant for a monophasic binding profile, K_A and K_B are intrinsic dissociation constants for two binding sites, and fract_A is the fraction of sites with dissociation constant K_A.

Acknowledgments

Correspondence should be addressed to A. G. E. We are indebted to Dr. Anthony Auerbach for providing the program MIL for kinetic analysis of our single-channel data. This work was supported by National Institutes of Health grants to S. M. S. (NS31744) and A. G. E. (NS6277), by a Muscular Distrophy Association research grant to A. G. E., and a MDA postdoctoral fellowship to K. O.

The costs of publication of this article were defrayed in part by the payment of page charges. This article must therefore be hereby marked *"advertisement"* in accordance with 18 USC Section 1734 solely to indicate this fact.

Received April 17, 1996; revised May 8, 1996.

References

Beeson, D., Brydson, M., and Newsom-Davis, J. (1989). Nucleotide sequence of human muscle acetylcholine receptor β subunit. Nucleic Acids Res. *17*, 4391.

Beeson, D., Brydson, M., Betty, M., Jeremiah, S., Povey, S., Vincent, A., and Newsom-Davis, J. (1993). Primary structure of the human muscle acetylcholine receptor. cDNA cloning of the gamma and epsilon subunits. Eur. J. Biochem. *215*, 229–238.

Blount, P., and Merlie, J.P. (1989). Molecular basis of the two nonequivalent ligand binding sites of the muscle nicotinic acetylcholine receptor. Neuron *3*, 349–357.

Blount, P., and Merlie, J.P. (1991). Characterization of an adult muscle acetylcholine receptor subunit by expression in fibroblasts. J. Biol. Chem. *266*, 14692–14696.

Bouzat, C., Bren, N., and Sine, S.M. (1994). Structural basis of the different gating kinetics of fetal and adult acetylcholine receptors. Neuron *13*, 1395–1402.

Changeux, J.P. (1990). Functional architecture and dynamics of the nicotinic acetylcholine receptor: an allosteric ligand gated channel. In Fida Research Foundation Neuroscience Award Lectures, Volume 4 (New York: Raven Press), pp. 21–168.

Chen, J., Zhang, Y., Akk, G., Sine, S., and Auerbach, A. (1995). Activation kinetics of recombinant mouse nicotinic acetylcholine receptors: mutations of α subunit tyrosine 190 affect both binding and gating. Biophys. J. *69*, 849–859.

Chiara, D., and Cohen, J. (1992). Identification of amino acids contributing to high and low affinity *d*-tubocurarine sites on the Torpedo nicotinic acetylcholine receptor subunits. Biophys. J. *61,* A106.

Colquhoun, D., and Sakmann, B. (1985). Fast events in single-channel currents activated by acetylcholine and its analogues at the frog muscle end plate. J. Physiol. (Lond.) *369*, 501–557.

Elmqvist, D., and Quastel, D.M.J. (1965). A quantitative study of endplate potentials in isolated human muscle. J. Physiol. (Lond.) *178*, 505–529.

Engel, A.G. (1994a). Quantitative morphological studies of muscle. In Myology: Basic and Clinical, Second Edition A.G. Engel and C. Franzini-Armstrong, eds. (New York: McGraw-Hill), pp. 1018–1045.

Engel, A.G. (1994b). Myasthenic syndromes. In Myology, Second Edition, A.G. Engel and C. Franzini-Armstrong, eds. (New York: McGraw-Hill), pp. 1798–1835.

Engel, A.G., Lindstrom, J.M., Lambert, E.H., and Lennon, V.A. (1977). Ultrastructural localization of the acetylcholine receptor in myasthenia gravis and in its experimental autoimmune model. Neurology *27*, 307–315.

Engel, A.G., Nagel, A., Walls, T.J., Harper, C.M., and Waisburg, H.A. (1993). Congenital myasthenic syndromes: I. Deficiency and short open-time of the acetylcholine receptor. Muscle. Nerve. *16*, 1284–1292.

Fu, D.-X., and Sine, S.M. (1994). Competitive antagonists bridge the α-γ subunit interface of the acetylcholine receptor through quaternary ammonium-aromatic interactions. J. Biol. Chem. *269*, 26152–26157.

Gehle, V.M., and Sumikawa, K. (1991). Site directed mutagenesis of the conserved N-glycosylation site on the nicotinic acetylcholine receptor subunits. Brain. Res. Mol. Brain. Res. *11*, 17–25.

Hamill, O.P., Marty, A., Neher, E., Sakmann, B., and Sigworth, F.J. (1981). Improved patch-clamp technique for high resolution current recording from cells and cell-free membrane patches. Pflügers Arch. *391*, 85–100.

Hongyo, T., Buzard, G.S., Calvert, R.J., and Weghorst, C.M. (1993). 'Cold SSCP': a simple, rapid and non-radioactive method for the optimized single-strand conformation polymorphism analyses. Nucleic Acids Res. *21*, 3637–3642.

Jackson, M.B. (1989). Perfection of a synaptic receptor: kinetics and energetics of the acetylcholine receptor. Proc. Natl. Acad. Sci. USA *86*, 2199–2203.

Katz, B., and Miledi, R. (1973). The binding of acetylcholine to receptors and its removal from the synaptic cleft. J. Physiol. (Lond.) *231*, 549–574.

Katz, B., and Thesleff, S. (1957). On the factors which determine the amplitude of the "miniature end-plate potential". J. Physiol. (Lond.) *137*, 267–278.

Kozak, M. (1987). An analysis of 5′-noncoding sequences from 699 vertebrate messenger RNAs. Nucleic. Acids Res. *15*, 8125–8148.

Lang, B., Newson-Davis, J., Prior, C., and Wray, D.W. (1983). Antibodies to motor nerve terminals: an electrophysiological study of a human myasthenic syndrome transferred to mouse. J. Physiol. (Lond.) *344*, 335–345.

Lee, B.S., Gunn, R.B., and Kopito, R.R. (1991). Functional differences among nonerythroid anion exchangers expressed in a transfected human cell line. J. Biol. Chem. *266*, 11448–11454.

Luther, M.A., Schoepfer, R., Whiting, P., Casey, B., Blatt, Y., Montal,

M., Montal, M.S., and Lindstrom, J. (1989). A muscle acetylcholine receptor is expressed in the human cerebellar meduloblastoma cell line TE671. J. Neurosci. *9*, 1082–1096.

Martin, A.R. (1966). Quantal nature of synaptic transmission. Physiol. Rev. *46*, 51–66.

Milone, M., Hutchinson, D.O., and Engel, A.G. (1994). Patch-clamp analysis of the properties of acetylcholine receptor channels at the normal human endplate. Muscle Nerve *17*, 1364–1369.

Mishina, M., Takai, T., Imoto, K., Noda, M., Takahashi, T., Numa, S., Methfessel, C., and Sakmann, B. (1986). Molecular distinction between fetal and adult forms of muscle acetylcholine receptor. Nature *321*, 406–411.

Ohno, K., Hutchinson, D.O., Milone, M., Brengman, J.M., Bouzat, C., Sine, S.M., and Engel, A.G. (1995a). Congenital myasthenic syndrome caused by prolonged acetylcholine receptor channel openings due to a mutation in the M2 domain of the ϵ subunit. Proc. Natl. Acad. Sci. USA *92*, 758–762.

Ohno, K., Hutchinson, D.O., Milone, M., Nakano, S., Hutchinson, D., Pruitt, J.N., Brengmann, J.M., Bren, N., Sieb, J., Sine, S.M., and Engel, A.G. (1995b). Molecular genetic basis of a slow channel syndrome. Muscle Nerve *18*, 463.

Ohno, K., Milone, M., Wang, H.-L., Nakano, S., Hutchinson, D., Pruitt, J. N., Brengmann, J.M., Bren, N., Sieb, J., Sine, S.M., and Engel, A.G. (1996). Identification of neuromuscular junction acetylcholine receptor mutations in the slow−channel congenital myasthenic syndrome. Neurology *46*, A214.

Qin, F., Auerbach, A., and Sachs, F. (1996). Estimating single-channel kinetic parameters from idealized patch-clamp data containing missed events. Biophys. J. *70*, 264–280.

Sambrook, J., Fritsch, E.F., and Maniatis, T. (1989). Molecular Cloning: A Laboratory Manual, Second Edition (Cold Spring Harbor, New York: Cold Spring Harbor Laboratory Press).

Schoepfer, R., Luther, M., and Lindstrom, J. (1988). The human medulablastoma cell line TE671 expresses a muscle-like acetylcholine receptor: cloning of the α subunit cDNA. FEBS Lett. *226*, 235–240.

Sigworth, F.J., and Sine, S.M. (1987). Data transformations for improved display and fitting of single-channel dwell time histograms. Biophys. J. *52*, 1047–1054.

Sine, S.M. (1993). Molecular dissection of subunit interfaces in the acetylcholine receptor: identification of residues that determine curare selectivity. Proc. Natl. Acad. Sci. USA *90*, 9436–9440.

Sine, S.M., and Claudio, T. (1991). γ- and δ-subunits regulate the affinity and the cooperativity of ligand binding to the acetylcholine receptor. J. Biol. Chem. *266*, 19369–19377.

Sine, S.M., and Taylor, P. (1979). Functional consequences of agonist-mediated state transitions in the cholinergic receptor. J. Biol. Chem. *254*, 3315–3325.

Sine, S.M., and Taylor, P. (1982). Local anesthetics and histrionicotoxin are allosteric inhibitors of the acetylcholine receptor. J. Biol. Chem. *257*, 8106–8114.

Sine, S.M., Claudio, T., and Sigworth, F.J. (1990). Activation of Torpedo acetylcholine receptors expressed in mouse fibroblasts: single-channel current kinetics reveal distinct agonist binding affinities. J. Gen. Physiol. *96*, 395–437.

Sine, S.M., Kreienkamp, H.-J., Bren, N., Maeda, R., and Taylor, P. (1995a). Molecular dissection of subunit interfaces in the acetylcholine receptor: identification of determinants of α-conotoxin M1 selectivity. Neuron *15*, 205–211.

Sine, S.M., Ohno, K., Bouzat, C., Auerbach, A., Milone, M., Pruitt, J. N., and Engel, A.G. (1995b). Mutation of the acetylcholine receptor α subunit causes a slow-channel myasthenic syndrome by enhancing agonist binding affinity. Neuron *15*, 229–239.

Thomsen, R.H., and Wilson, D.F. (1983). Effect of 4-aminopyridine and 3,4−diaminopyridine on transmitter release at the neuromuscular junction. J. Pharmacol. Exp. Ther. *227*, 260–265.

Uchitel, O., Engel, A.G., Walls, T.J., Nagel, A., Atassi, Z.M., and Bril, V. (1993). Congenital myasthenic syndromes. II. Syndrome attributed to abnormal interaction of acetylcholine with its receptor. Muscle Nerve *16*, 1293–1301.

Upender, M., Raj, L., and Weir, M. (1995). Megaprimer method for in vitro mutagenesis using parallel templates. Biotechniques *18*, 29–30.

Weiland, G., Georgia, B., Lappi, S., Chignell, C., and Taylor, P. (1977). Kinetics of agonist-mediated transitions in state of the cholinergic receptor. J. Biol. Chem. *252*, 7648–7656.

Zhang, Y., Chen J., and Auerbach, A. (1995). Activation of recombinant mouse acetylcholine receptors by acetylcholine, carbamylcholine and tetramethylammonium. J. Physiol. *486*, 189–206.